Heat transfer performance analysis of a novel circular microchannel heat sink

Saichen Ma *

Department of mechanical engineering, University of Shanghai for Science and Technology

* Corresponding Author Email: saichen.ma@hs-furtwangen.de

Abstract. Electronic component heat dissipation is a significant issue in the development of electronic equipment. A unique circular micro-channel heat sink is proposed in this study. Cylinders and cones are evenly arranged inside the micro-channel to change the flow state of the liquid. Using the fluid analysis Fluent to calculate and simulate the heat sink, the pressure distribution and flow velocity distribution in the heat sink are obtained. The temperature field of the heat sink during operation is obtained through the Steady-State Thermal simulation, and the heat transfer performance of the heat sink is determined. The results indicate that the microchannel structure proposed in this research has great heat transfer performance.

Keywords: Electronic Components, Micro-Channel Heat Sink, Heat-Fluid-Solid Coupling, Heat Transfer Performance

1. Introduction

Electronic components need to work under the drive of electric power, but the conversion efficiency of energy cannot reach 100% conversion. The rest is converted into heat, which makes the working environment of electronic devices and electronic equipment overheated. Therefore, electronic components need to be cooled during being used. As the development of CUP chips, the heat generation of electronic chips during work continues to increase. It exceeds the limits of traditional air-cooling technology. Therefore a more efficient cooling technique needs to be applied. Nowadays many researchers have studied microchannel heat sinks, and have developed many new types of microchannel heat sink structures, which can improve the heat dissipation rate of electronic components.

The concept of microchannel heat sink was proposed by Tuckerman and Pease in 1981 by 1985. Since then, more and more scholars have begun to study the micro-channel heat sink structure to improve the heat transfer performance. Zhang Minghui [1] analyzed the structure of straight microchannels with circular section, and discussed the influence of parameters on flow heat transfer. Xia Guodong, Chai Lei [2] conducted an experimental on the heat transfer and fluid flow of the trapezoidal cross-section silicon-based micro-channel heat sink structure. The research team of H.A. Mohammed [3] studied the effect of wave shapes of various amplitudes on heat transfer. Hong F and Cheng P [4] conducted a 3D numerical analysis of a finned microchannel (finned microchannel) to discuss its enhanced heat transfer mechanism. The research team of Xia GuoDong [5] studied the entropy generation and heat transfer characteristics in the microchannels of the fan-shaped cavity and inner rib. Zhai Yuling, Xia Guodong [6-7] and others conducted a numerical simulation study on the fluid flow and heat transfer of the spaced fan-shaped cavity micro-channel proposed by Chai. Navin Raja Kuppusamy [8] conducted a numerical on the secondary flow microchannel.

A unique micro-channel heat sink structure is developed in this study, and the thermal performance of the heat sink structure is evaluated using a numerical simulation method. Firstly, the 3D modeling of the new heat sink structure is carried out by UG software. Then the fluid analysis software Fluent and the steady-state thermal analysis software Steady-state thermal is used to analyze the heat transfer performance of the micro-channel heat sink.

2. Physical model

The structure proposed in this research is designed based on the circular section microchannel. For circular microchannels, it is characterized in that the cross-sectional shape of the microchannel is a commonly used circular cross-section. Generally, the fluid in the circular microchannel is a laminar flow, and the heat exchange rate of the fluid in the channel is relatively stable. Figure 1 shows the general structure of the micro-channel heat sink suggested in this study.

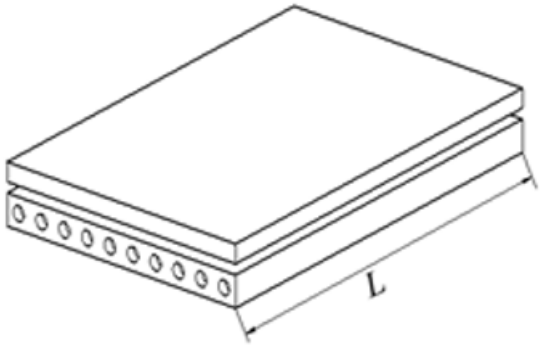


Figure 1. Structure of heat sink system

The heat sink's interior features a cone-shaped construction, and the cones are evenly distributed in the channel. UG software is used to model one of the channels in the overall structure, Fig 2.

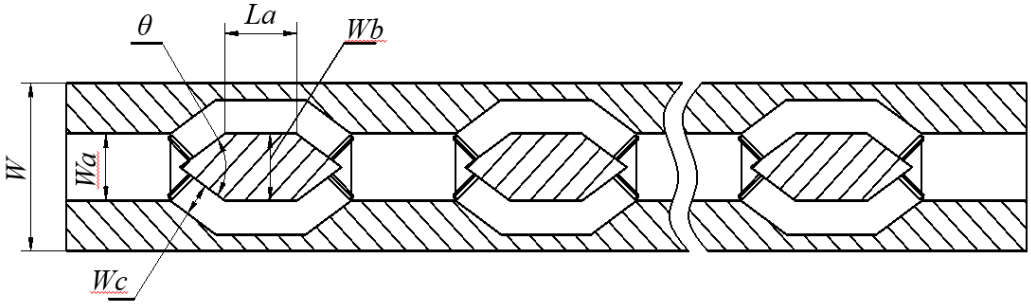


Figure 2. Single microchannel

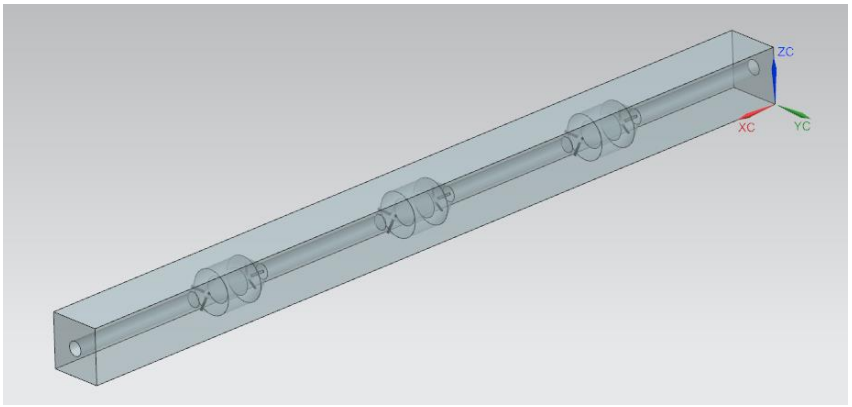


Figure 3. Cross-sectional view of a single micro-channel heat sink structure

The cross-sectional view of the single micro-channel heat sink structure is as Figure 3. The structural parameters of the are shown in Table 1.

Liquid inlet aperture (*Wa*), Shunt channel width (*Wc*), Cone angle (*θ*), Cone length *(La*), Cone width (*Wb*), Shunt outer diameter (*W*)

Table.1. Structure parameters

θ/°	*Wb*/mm	*La*/mm	*Wa*/mm	*S*	*W*/mm	*Wc*/mm
68°	0.70	0.65	0.40	3	1.2	0.325

The fluid medium enters the channel from the liquid inlet, then split into the split channel when it flows through the cone column, it finally merges at the other end of the cone angle. The uniform distribution of the cones can make the fluid obtain periodic splitting and confluence. When the fluid enters the heat sink, the core layers with lower temperature are divided and reunited. Thus, the fluid can conduct sufficient heat exchange at low temperature, thereby improving the heat exchange performance.

3. Governing Equations for Flow and Heat Transfer

For MEMS with equivalent diameters in the range of 1 μm to 1 mm, the continuum assumption and N-S equation are still applicable [9]. Heat conduction according to Fourier's law applies under the condition that the characteristic length of the object is way larger than the mean free path of the heat-carrying particles.

For microchannel heat sinks, the heat generated by the electronic components is transferred to the walls of the heat sink channels, which are then carried away by the coolant through convective heat transfer. The following assumptions are made to simplify the analysis:

(1) Steady-state flow and heat transfer process
(2) Ignore wall roughness
(3) The fluid in the heat sink is an incompressible fluid
(4) The thermophysical properties of solids and liquids remain unchanged

The fluid governing equation:

① The fluid's continuity equation:

$$\frac{\partial u}{\partial x}+\frac{\partial v}{\partial y}+\frac{\partial w}{\partial z}=0 \tag{1}$$

② The fluid's momentum conservation equation:

$$\rho(u\frac{\partial u}{\partial x}+v\frac{\partial u}{\partial y}+w\frac{\partial u}{\partial z})=F_x-\frac{\partial p}{\partial x}+\eta\left(u\frac{\partial^2 u}{\partial x^2}+v\frac{\partial^2 u}{\partial y^2}+w\frac{\partial^2 u}{\partial z^2}\right) \tag{2}$$

$$\rho(u\frac{\partial u}{\partial x}+v\frac{\partial u}{\partial y}+w\frac{\partial u}{\partial z})=F_x-\frac{\partial p}{\partial y}+\eta\left(u\frac{\partial^2 u}{\partial x^2}+v\frac{\partial^2 u}{\partial y^2}+w\frac{\partial^2 u}{\partial z^2}\right) \tag{3}$$

$$\rho(u\frac{\partial u}{\partial x}+v\frac{\partial u}{\partial y}+w\frac{\partial u}{\partial z})=F_x-\frac{\partial p}{\partial z}+\eta\left(u\frac{\partial^2 u}{\partial x^2}+v\frac{\partial^2 u}{\partial y^2}+w\frac{\partial^2 u}{\partial z^2}\right) \tag{4}$$

③ The energy conservation equation of fluid :

$$\rho\cdot C_p(u\frac{\partial T}{\partial x}+v\frac{\partial T}{\partial y}+w\frac{\partial T}{\partial z})=\lambda_l\left(u\frac{\partial^2 T}{\partial x^2}+v\frac{\partial^2 T}{\partial y^2}+w\frac{\partial^2 T}{\partial z^2}\right) \tag{5}$$

The components of fluid velocity in the *x*, *y*, *z* directions are u, *v*, *w* (m/s)

The energy equation of the solid part :

$$\lambda_s\left(u\frac{\partial T}{\partial x^2}+v\frac{\partial T}{\partial y^2}+w\frac{\partial T}{\partial z^2}\right)=0 \tag{6}$$

4. Heat transfer performance analysis

The heat transmission performance of the heat sink is investigated using a numerical simulation method in this study. The pressure and flow velocity distribution of the fluid in the heat sink are obtained by Fluent calculation and simulation. The temperature field of the heat sink during operation is obtained through the Steady-State Thermal simulation. Under thermal load, the base temperature of the heat sink structure is determined intuitively. The heat transfer performance is determined according to the results of numerical simulation.

4.1. Boundary conditions

In traditional fluid mechanics analysis, no-slip boundary conditions are used in the momentum equation of the fluid. The no-temperature jump boundary condition is used in the energy equation. For gases, when Kn < 0.001 (Kn is defined as the ratio of the molecular mean free path to the characteristic flow size), the prediction results obtained under the no-slip condition and the no-jump condition are relatively accurate [10]. For the heat sink studied in this research, the air is at normal temperature and pressure, Kn<0.00065, the liquid mean free path is way smaller than the gas mean free path. Therefore, the no-slip boundary conditions and the no-jump boundary can be applied. Symmetrical boundary conditions are used around the model.

At the liquid heat sink inlet, the flow velocity is a known flow velocity, which is set to 1.5m/s (the Reynolds number of the liquid inlet Re=1039.79).

The room temperature is set to 20°C. The initial temperature of the medium fluid introduced is also 20°C. The area of the heat sink that comes into contact with the electronic components is a uniform constant heat flow. The heat flow density released by the electronic components to the heat sink is 1W/mm^2. Except for the heat load loading surface, the convective heat transfer coefficient between the wall area of the heat sink and the air is 10^{-5}W/mm^2.

Silicon is used to construct the micro-channel heat sink while deionized water is as the passing medium. Table 2 shows the thermophysical parameters of solid and liquid materials involved in adding materials:

Table.2. Material performance parameters

Physical quantity	Deionized water	Silicon
Thermal Conductivity k $\left(W \cdot m^{-1} \cdot k^{-1}\right)$	$-0.58166 + 6.3556 \times 10^{-3}T - 7.964 \times 10^{-6}T^2$	0.21
Specific heat **Cp** $\left(J \cdot kg^{-1} \cdot k^{-1}\right)$	4187	703
Density **ρ** $(kg \cdot m^{-3})$	998.2	2330

4.2. Meshing

Mesh the entire heat sink model in Fluent, set the mesh quality to Medium. A total of 459,245 nodes and 2,437,187 meshes were generated. The enlarged mesh division of the model and the number of meshes generated are shown in Figures 4 and 5.

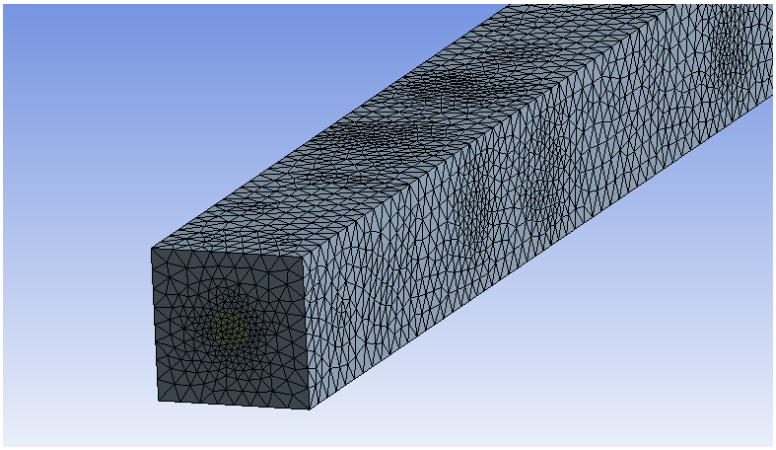


Figure 4. Mesh division diagram

Statistics	
Nodes	459245
Elements	2437187
Mesh Metric	None

Figure 5. Statistics of the number of nodes and the number of grids

4.3. Calculation method

First, use Fluent to analyze the fluid to obtain the pressure and flow velocity distribution of the fluid in the heat sink; then import the solution result of Fluent into Steady-State Thermal as its solution condition. After applying the thermal load and the convection coefficient with the air, the temperature field distribution of the heat sink is calculated.

The solver in Fluent selects a separate solver (Pressure-based), the pressure-velocity coupling equation adopts the SIMPLE algorithm, and the discrete method selects the first order upwind. In the fluid model option, select the fluid model according to the calculated Reynolds number Re. Set the speed accuracy and energy calculation accuracy in the x, y, and z directions in the iterative calculation to 10^{-4}, and set the number of iterative calculations to 1000 times before the calculation. The convergence accuracy of the iterations is 10^{-6}.

In the steady-state thermal analysis, it is necessary to load the heat flux density on the surface of the heat sink in contact with the electronic components. The heat flux density loading surface is shown in Figure 6. The loaded heat flux value was $1W/mm^2$. Except for the contact surface between heat sink and electronic components, convective heat transfer coefficient between heat sink and air is set to $10^{-5}W/mm^2$ for the other 5 walls.

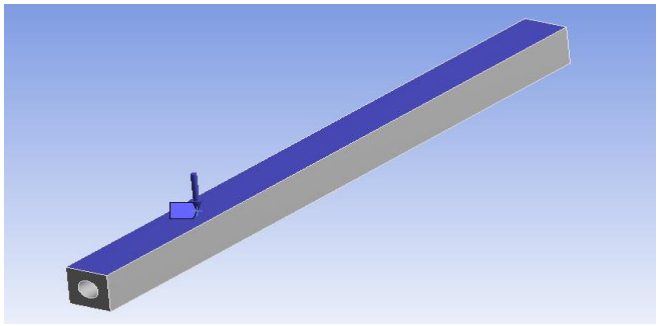


Figure 6. Schematic diagram of thermal load loading surface

4.4. Pressure Analysis of Fluid

Through Fluent, the fluid pressure distribution of the fluid in the XZ plane at -1/2 of the Y-axis direction is shown in Figure 7. It can be known that if the atmospheric pressure is 0 Pa, the fluid pressure gradually decreases with the flow of the fluid. The fluid pressure at the liquid outlet is the

smallest which is -1.31×10^{1} Pa. The maximum pressure appears at the liquid inlet which is 1.31×10^{4}Pa.

There is a small increase in the pressure value of the fluid near the tip of the cone angle. This is because the fluid is hindered by the tip of the cone, which breaks the flow rule of the fluid along the straight channel. Under the obstruction of the cone angle, the flow rate decreases, and the dynamic pressure is converted into static pressure. As a result, the pressure value near the cone's tip rises. A similar phenomenon occurs in the first two cone-column structures, but at the last cone-column structure, due to the continuous reduction of fluid pressure, the dynamic pressure conversion at the cone angle is low, which is not sufficient for supercharging.

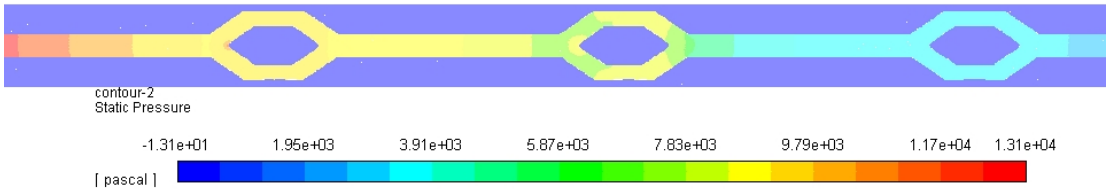


Figure 7. Pressure nephogram of fluid in heat sink

4.5. Velocity Analysis of Fluid

The fluid velocity nephogram of the XZ plane of the fluid at -1/2 of the Y-axis direction of the heat sink can be seen in Fig8. The flow velocity of the fluid in the straight channel increased to a maximum of 2.25m/s, and the velocity began to decrease significantly to about 1.5m/s after the diversion at the cone angle, indicating that the fluid was hindered at the tip of the cone angle. The velocity reaches the lowest value of about 0.675m/s at the outer diameter channel of the split flow, and converges at the other end of the cone, then the velocity begins to rise. This flow rate variation law appears at each section of the cone-column structure.

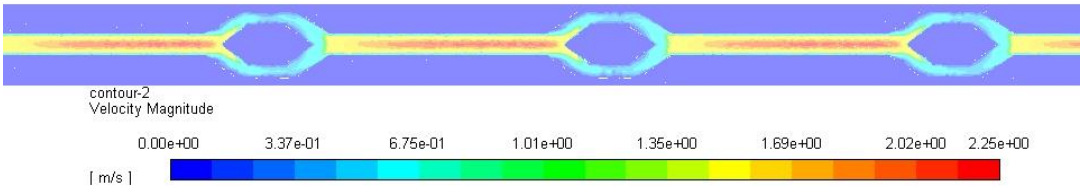


Figure 8. Velocity nephogram in heat sink

Five detection points in different regions are taken near the first cone-column structure in the channel, and the fluid state of the region where each point is located is analyzed. The point selection is in Fig 9. The fluid velocity as well as the Reynolds number Re at each point is calculated by Fluent. The fluid flow state of the fluid at each point is judged.

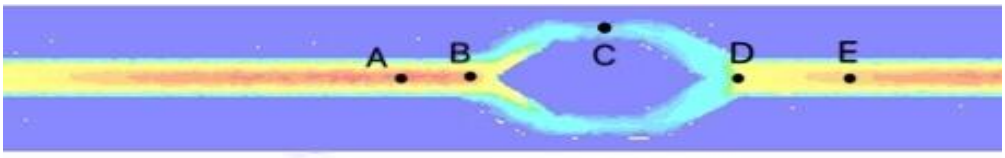


Figure 9. Points diagram

Table 3. Coordinate, velocity and Reynolds number of each point

	Coordinate	Velocity m·s-1	Re
A	(3.2546,-0.725,0.75)	1.957	781.9740811
B	(4.3111,-0.725,0.9)	1.634	646.959822
C	(5.6286,-0.725,1.2)	0.431	170.648521
D	(6.3972,-0.725,0.9)	1.339	530.1586301
E	(7.5972,-0.725,0.75)	2.159	854.8263499

When the Reynolds number Re is less than 2300, the fluid flow state is laminar flow. When 2300 < Re < 4000, the fluid is in transition state. When Re > 4000, the fluid flow state is turbulent. From calculation results in table3, it can be known that the flow state of the fluid in the channel is laminar flow.

4.6. Heat sink temperature analysis

The temperature field distribution during operation is obtained through thermal steady state analysis, in Fig10. The maximum temperature value of the heat sink is 32.51℃, and the minimum temperature value is 19.845℃. The maximum temperature is found on the contact area between the electrical components and the heat sink. This maximum temperature is named as the substrate temperature.

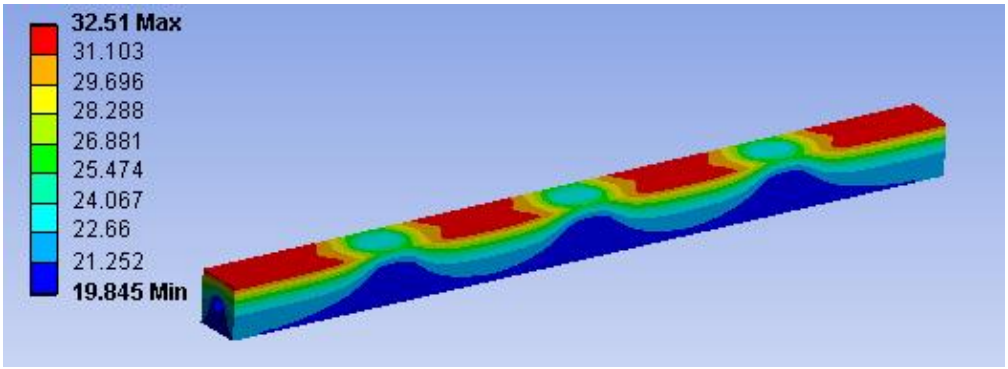


Figure 10. Heat sink temperature nephogram

It can be seen from the structure that the uniformly distributed cone-column structure makes uniformly distributed low temperature areas appear on the contact surface between electronic components and heat sink. At the same time, from the temperature field distribution on the sidewall of the heat sink it turns out that the fluid splitting at the cone-column structure makes the temperature distribution on the sidewall of the heat sink significantly different from that at the straight channel. The temperature distribution at the straight channel tends to be horizontal; while the low temperature area in the temperature distribution field at the cone column is relatively large, and the heated area is relatively concentrated in the upper half of the heat sink. This is because after the fluid is split at the cone, the heat exchange area in outer diameter channel of split increases, which increases the heat exchange. The heat exchange of the fluid at the cone is greater than that in the straight channel at the same time.

5. Conclusion

(1) The conical-column structure can divide the fluid, so that the core layer with lower temperature can conduct sufficient heat exchange.

(2) The fluid pressure in the heat sink channel gradually decreases with the flow of the fluid. The inlet pressure of the fluid at is the largest. When the fluid flows near the cone angle of the cone, it is hindered by the cone angle, and the dynamic pressure is converted into static pressure, so a pressurized area appears near the cone angle.

(3) The straight channel in the heat sink channel has a faster fluid flow velocity. As the change in displacement, the flow velocity progressively increases until it reaches its maximum value. After the fluid passes through the taper column, the flow velocity begins to decrease, and the flow velocity in the shunt outer diameter channel reaches the minimum value. The fluid velocity gradually increases after the confluence at the other end of the cone. By calculating the fluid Reynolds number Re, it is concluded that the flow state of the fluid in the channel is laminar flow.

(4) The cone-column structure increases the heat exchange area in the heat sink, improves the heat transfer performance of the heat sink, and makes the cone-column corresponding to the contact surface to have a distinct low temperature area. It can be seen from the side wall surface of the heat sink that the temperature change is concentrated in the upper half of the heat sink.

References

[1] Zhang Minghui. Numerical study on heat transfer characteristics of circular microchannel heat sink flow [J]. Building Thermal Energy Ventilation and Air Conditioning, 2009, 28(01): 10-13.

[2] Xia Guodong, Chai Lei, Qi Jingzhi. Study on fluid flow and heat transfer characteristics of trapezoidal silicon-based microchannel heat sink [J]. Journal of Beijing University of Technology, 2011, 37(7): 1079-1084.

[3] Mohammed H. A, Gunnasegaran P., Shuaib N. H. Numerical simulation of heat transfer enhancement in wavy microchannel heat sink [J]. International Communications in Heat and Mass Transfer, 2011, 38(1): 63-68.

[4] Hong F., Cheng P. Three dimensional numerical analyses and optimization of offset strip-fin microchannel heat sinks [J]. International Communications in Heat and Mass Transfer, 2009, 36(7): 651-656.

[5] Xia Guodong, Zhai Yuling, Cui Zhenzhen. Characteristics of entropy generation and heat transfer in a microchannel with fan-shaped reentrant cavities and internal ribs [J]. Science China(Technological Sciences), 2013, 56(07): 1629-1635.

[6] Zhai Yuling, Xia Guodong, Cui Zhenzhen. Numerical simulation of flow and heat transfer in spaced fan-shaped cavity microchannels [J]. Journal of Beijing University of Technology, 2014, 40(4): 627-633.

[7] Zhai Yuling, Xia Guodong, Liu Xianfei. Thermodynamic Analysis of Heat Transfer Process of Complex Microchannel Heat Sink Liquid Enhancement [J]. Chinese Journal of Chemical Engineering, 2014, 65(09): 3403-3409.

[8] Navin R., Saidur N. Numerical study of thermal enhancement in micro channel heat sink with secondary flow [J]. International Journal of Heat and Mass Transfer, 2014, 78: 216-223.

[9] Zeng Yuan. Effect on Single-phase Channel Flow and Heat Transfer at Microscale [J]. International Journal of Heat and Fluid Flow. 2003, 24: 284-298.

[10] Liu Jing. Micro/nano-scale heat transfer [M]. Science Press, 2002: 145-220.